D.3.5.1 – 3.5.2 – Model able to map the risk and based future scenario & Regional high-resolution map of vulnerability

Document Control Sheet

Project number:	10048765
Project acronym	ASTERIS
Project Title	Adaptation to Saltwater inTrusion in sEa level RIse Scenarios
Start of the project	January 2019
Duration	24 months

Related activity:	3.5 – Development of a model of the risk based on future scenarios
Deliverable name:	D.3.5.1 – Publication of a model able to map the risk and based on future scenarios 3.5.2- Regional high-resolution maps of vulnerability
Type of deliverable	Report
Language	English
Work Package Title	Modelling present and future salt ingression in Adriatic coastal aquifers
Work Package number	3
Work Package Leader	University of Urbino “Carlo Bo” – (UNIURB)

Status	Final
Author (s)	Gaia Galassi (UNIURB) Simone Galeotti (UNIURB) Giorgio Spada (UNIBO)
Version	1
Due date of deliverable	31 December 2020
Delivery date	31 December 2020

INDEX

1. INTRODUCTION

The Adriatic region is highly vulnerable to the adverse impacts of climate change. Between climate-related impacts that could affect the coastal area, in last years the relevance of salt intrusion is increased. Coastal aquifers are characterized by a natural gradient towards the seaboard, where groundwater discharges into the sea. A saline wedge normally exists below lighter freshwater.

The interface between freshwater and heavier seawater is in a state of dynamic equilibrium and the interface is a transition zone of mixed salinity. This equilibrium can be affected from multiple directions: from above due to inundation or storm surge, laterally due to encroachment of the freshwater/saltwater interface, and from below due to upcoming of saline groundwater caused by pumping (Klassen, and Allen, 2016).

The Italian and Croatian coasts are subject to the influences of touristic pressure, entailing the increasing extraction of groundwater in peak periods, and its effect on salt ingression, as well as the effects of pumping for agriculture during drought, which are often not taken into account in the management plan for water catchment.

In addition, climate change is exacerbating processes affecting salt intrusion; in particular, sea level rise (forced by changes to atmospheric pressure, thermal expansion of oceans and seas and melting of ice sheets and glaciers) is one potentially significant process that is expected to play a role in sea water intrusion (Werner et al., 2009).

In this context, it is important to understand the potential risk of salt ingression in coastal aquifers.

Plans for groundwater resource management demand a realistic estimate of future local sea level response for a range of the most likely to the worst-case scenarios of global warming. It is, therefore, imperative understanding the interaction between fresh groundwater and seawater intrusion in a sea-level rise perspective to achieve a sustainable management of coastal water resources.

This work aims to obtain a conceptual model for the risk assessment to salt intrusion in North Adriatic basin for future scenarios of climate change (Collins et al., 2013). Different works exist that have assessed the risk of salt intrusion at local level. This work is extended to a broad area (almost 2000 km of coasts), involving three Countries (Italy, Croatia and the short portion of

Slovenia facing Adriatic coast) and including a variety of geological, morphological and also socioeconomical conditions.

This deliverable contains also the map of risk of salt o salt intrusion in in coastal aquifer for future scenarios of climate change. The map is referred to the North Adriatic basin. The map represents a tool for the administration in the decision of authorising further water extraction and in comparing different locations.

2. Basic structure of the model

The assessment of risk of salinisation has to simultaneously consider vulnerability (that embeds also the probability of occurrence) and the potential loss (defined as economic consequences due to the contamination of groundwater supply, impacts on human health due to well contamination, or multiple consequences on ecological systems). According to Simpson et al. (2014), the equation of risk assessments reads:

$$Risk\ (R) = Vulnerability\ (V) * Loss\ (L) \qquad (1)$$

where the vulnerability is defined as aquifer susceptibility and hazard threat, and the probability of occurrence is attributed to each hazard threats:

$$Vulnerability\ (V_A) = Aquifer\ susceptibility\ (S_A) * hazard\ threat\ (T_H) \qquad (2)$$

Following the scheme proposed by Klassen, and Allen (2016), we propose the following scheme for modelling risk of salt ingression in coastal aquifer.

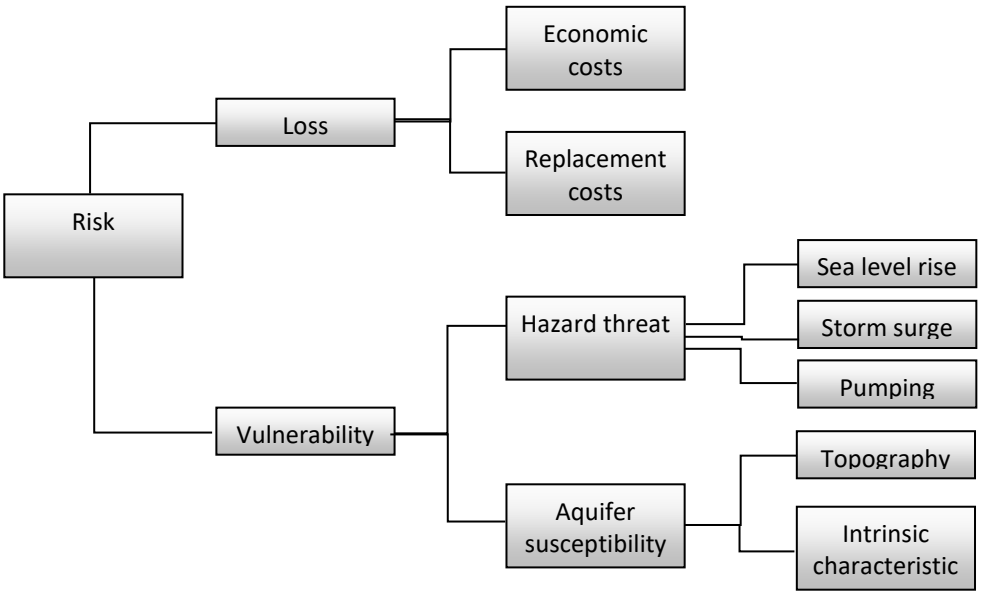

Figure 1: Scheme for modelling risk of salt ingression of coastal aquifers.

Aquifer susceptibility has been analysed in activity 3.2. It is not time dependent for the time scale of the analysis (less than a century).

For Hazard threats, Sea level rise has been modelled at 2100, also based on the result of activity 3.3. Storme surge scenarios have been also included here.

Pumping can not be modelled as future scenario, since it will depend not only by the current presence of wells, but also by the evolution of economic context (which acts on the need of water resources and hence on the intensity of pumping) and by the political and administrative choice related to use of water resources. For this reason pumping is not introduced in the model as an input, but as a variable.

In this way, model output will not simply be a static map containing information about risk, but instead will produce a dynamic tool to address government's choices about water resource use, by comparing alternatives in planning.

The loss, especially in terms of economic loss, is not simple to evaluate and project for the future, in a broad scale analysis. Nevertheless, a parameter associated to the use of soil has been introduced as proxy of need of restoration coast.

For the combination of the different components of vulnerability (aquifer susceptibility S_A and Hazard threats H_T) and Loss, following the approach delineated by Eriksson et al. (2018), a

system of weight has been introduced. Using Eq. (1) and (2) we obtain

$$R = \sum_{i=1}^{n} S_{Ai} \cdot W_i \times \sum_{j=1}^{n} H_{Tj} \cdot W_j \times \sum_{k=1}^{n} L_k \cdot W_k \qquad (3)$$

where *i, j* and *k* are referred to the componente of risk for aquifer susceptibility, hazard threats and Loss, respectively, and $W_{i,j,k}$ are the associated weights.

For the assessment of each component of S_A, H_T and L, the parameters contributing to each variable introduced in the model have been associated to a rank (from 1, very low, to 5, very hight).

The analysis use GIS (Geographic Information System) tools. All available information have been included as layer in the model. The analysis has been performed along a 5 km buffer from the coast to the interior. We used a grid of 1 km X 1 km to analyse and combine the considered parameters. The equation (3) is then applied at mapping unit level.

3. Assessing vulnerability

3.1. Aquifer susceptibility

To assess the risk component deriving from aquifer susceptibility, both intrinsic characteristics and topography have been considered. The intrinsic characteristics are base on hydrogeology, and specifically on lithology and aquifer type. For topography, both elevation and distance from coast have been considered.

The information obtained for the two variables has been arranged to create a possible scenario of susceptibility, using the following system of weights:

- elevation: W= 0.25;
- Distance from coast: W= 0.25;

- Hydrology: W= 0.50;

The weights have been allocated to balances uniformly all the variables, considering that:

- for hydrogeology, the rank accounts for two interdependent variables, namely aquifer type and lithology;
- Elevation and distance are two not completely independent variables.

Applying the first parts of Eq. (3) the component of vulnerability deriving from aquifer susceptibility, reads:

$$S_A = 0.25 \cdot El + 0.25 \cdot D_C + 0.5 \cdot Hy \quad (4)$$

3.1.1 Topography

Topographic **elevation** has been considered as a parameter for the characterisation of vulnerability of coastal aquifer in many works (see, i.e. Kennedy, 2012, Eriksson et al., 2017). Other authors (i.e. Klassen and Allen, 2016) use slope instead of elevation. Given the broad scale of the map and the complexity of coastal morphology, here we choose elevation as the most appropriate parameter.

The rating for the assessment of vulnerability for elevation and distance form coast is listed in table 1. Differently from Eriksson et al. (2017), who identified three classes of elevation, with maximum height 10 m.s.l.m., here, to account also for the low risks, we chose 5 classes, ranging from 0 to over 500 m.s.l.s.. Data are derived from the Copernicus database, and pertain to the EU-DEM v.10 products.

As an additional parameter, the distance from the coast is considered. This information is obtained drafting subsequent buffers from the coast. Value of distance have been extended compared to Klassen and Allen (2016), in order to account for the regional dimension of this work as well as to consider lower risk results.

Table 1: Ranks for vulnerability assessment for topography

Rating	Elevation	Distance from coast
5	< 10	0-50
4	10 - 50	50-250
3	50 -100	250-500
2	100 - 200	500-1000
1	200 - 500	1000-1500
0	> 500	>1500

3.1.2 Intrinsic characteristics

To assess the intrinsic characteristics of aquifers, different rating of vulnerability have been attributed to **hydrogeology**. Data are from the International Hydrogeological Map of Europe from Federal Institute for Geosciences and Natural Resources[1]. The final rating, ranging from 1 to 5, results from the combination (average rounded at the upper bound) of the ranking of two parameter: **aquifer type** and **lithology**.

Table 2: Ranks for vulnerability assessment for aquifer types

Aquifer type	Rating	Lithology (L3)
Highly productive fissured aquifers (including karstified rocks)	5	Gravel Limestones Limestones and marls Marbles
High productive aquifer	4	Quartzites Sands
Low and moderately productive fissured aquifers (including karstified rocks) Low and moderately productive porous aquifers	3	Marlstones and sands Sandstones and marls

[1] https://www.bgr.bund.de/ihme1500

Locally aquiferous rocks, porous or fissured	2	Clays Sandstones and clays
Practically non-aquiferous rocks, porous or fissured	1	

3.2 Hazard threats

For hazard threats, information on sea level rise and storm surge projection is introduced in the model. In analysing hazard threats it is also necessary to include pumping: even if in this model, pumping is introduced as an open variable and not as layer, it is taken in equation (3) for the H_T component.

The system of weight chosen is then:

- storme surge: W= 0.35;
- sea level rise: W=0.35
- Pumping from wells: W=0.30.

Equation (3) for H_T then reads:

$$H_T = 0.35 \cdot Sl + 0.35 \cdot SS_L + 0.30 \cdot P_W \quad (5)$$

where *Sl* and SS_L are sea level rise and storm surge level, respectively, and P_W accounts for pumping from wells. As first approximation, in the computation of eq. (5) Pw is considered equal to 1. Real value of Pw can be introduced in applying the model at low scale level (see section 5).

3.2.1 Sea level rise

Sea level rise is a key parameter in analysing salt ingression in coastal aquifer, since it will move the transition zone of freshwater and saltwater inland, increasing the risk of saltwater intrusion for inland wells (Eriksson et. Al, 2018).

The long-term sea-level variations at a given place and time stem from the combination of several contributions. Assuming that these are acting independently, following the general approach outlined by Mitrovica et al. (2001), the total variation is given by the combination of different factors including GIA component of sea-level change, the contribution associated with mass exchange (referred to the current melting of terrestrial ice masses), the component due to

the ocean response (this includes the ocean circulation contributions and thermosteric plus halosteric effects), the contribution of other factors (including, for instance, sediment compaction, co- and post-seismic deformations and other tectonic effects). To obtain scenarios for the evolution of future sea level, all these components have to be modeled. A first attempt of future sea-level scenarios at 2050 for Mediterranean Sea was presented by Galassi and Spada (2014); here their work is expanded to develop sea-level scenarios to 2100.
The AR5 IPCC report analyzed different Representative Concentration Pathway (RCP) pathways, i.e. greenhouse gas concentration trajectory, to which correspond sea-level scenarios at 2100. Among those published, we have considered RCP4.5 (intermediate scenario, with peak around 2040) and RCP8.5 (continued growth of gas emissions) to estimate a possible upper bound of future RSL variation in the study area. For that reason, both steric and current ice melting component of sea level, have been modeled according to the RCP 4.5 and RCP 8.5. The GIA component is not influenced by the current evolution of climate and it is independent from scenarios.

The **geodynamic components of sea level** account for the deformation of solid Earth as consequence of ice melting. Here two different geodynamical processes are taken into consideration: the current melting of the ice sheets, glaciers and ice caps and the Glacial Isostatic effects deriving from the melting of ice at Last Glacial maximum. For both, sea-level projections have been modeled with the aid of an improved version of program SELEN (Spada and Melini, 2019), which solves the “sea-level equation” (Farrell and Clark, 1976) assuming a spherically symmetric, rotating, elastic and isotropic Earth model, with a PREM structure.

The glacial isostatic adjustment (GIA) component of sea-level change is originated by the ongoing mass redistribution still caused by the melting of the late-Pleistocene ice sheets. GIA effects average to zero across the surface of the oceans, but they will be the source of local and regional sea-level variations, both in the formerly glaciated areas at the Last Glacial Maximum (LGM, ~ 21,000 years ago) and in key-areas such as the Mediterranean Sea (Galassi and Spada, 2014). The pattern of the sea-level change expected from future mass loss from glacial and ice caps and continental ice sheets shows significant variations even at the 100-km spatial scale (Spada et al., 2013). To model GIA effects, it will make use of the gravitationally

self-consistent Sea Level Equation formalism and account for solid Earth deformations, gravitational and rotational perturbations. GIA is estimated by the ICE-6G (VM5a) global model of Peltier et al. (2013).

Sea level is also influenced by the effect of the current terrestrial melting (hereinafter TIM) of glaciers, ice caps (GIC), and ice sheets (Antarctica - AIS - and Greenland - GIS). For the AIS and the GIS, the surface mass balance (SMB) and the ice dynamic (DYN) components of TIM are considered separately. The projection of melting of glaciers and ice caps has been taken from Slangen et al (2014). The glacier estimate is computed using CMIP5-based projections of temperature and precipitation changes over glaciered regions in combination with a glacier area inventory (Radi´c and Hock 2010) in a model for glacier mass loss that is based on volume-area considerations (Slangen and van de Wal, 2011). The SMB change have been combined with the projected CMIP5 global mean surface temperature change to calculate the CMIP5-SMB. Since ice-melting dynamical processes are complex (accounting for calving and melt of marine-terminating glaciers, ice flow-SMB feedback, melting of ice shelves from below for changes in circulation cause warmer water, etc.), the projection modeled by Slangen et al (2014) uses an RCP-independent scenario bounded by two different estimates: a lower bound taken from a scaled-up estimate of IPCC AR4, and upper bound corresponding to the estimates presented in Katsman et al. (2011). For this project, the TIM mass balance included in the model is that projected according to the scenarios A and B described in Slangen (2014), corresponding to the RCP 4.5 and 8.5 of IPCC, respectively; the model has been developed accordingly with Spada et al. (2013), to obtain sea-level pattern (fingerprint) at 2100.

For the **steric component** of sea - level, data from MEDCORDEX experiment (Ruti et al, 2016) have been used. In order to account of all the component not depending on the geodynamic deformations, the variable considered is the sea surface height above geoid. This variable accounts for sea surface height fluctuations through different seasons due to thermal expansion and contraction, and variations caused by other factors such as the wind and tides. It is referred to the reference level (the geoid), representing the sea surface height when no external factors are taken into consideration. Data used derived are based on CNRM-CM5 General Circulation Model, CNRM-RCSM4 v1 regional Circulation Model, and CMIP5 Ensemble Members r8i1p1. Results for RCP 4.5 and RCP 8.5 have been extracted. Monthly data have been averaged for the two reference period 2011-2020 (2015 central year) and 2091-2100, and the difference

between the two period, computed.

Information on sea level rise are then combined to obtain an overall projection at 2100. To assess the maximum risk, only the RCP 8.5 has been considered in the model.
According with Ghyben–Herzberg formula, there is a relation between saltwater intrusion and the ratio between the two thickness of freshwater zones above and below sea level. Sea level rise influences groundwater hydraulics change this ratio, in a linear way.
An almost linear dependency of salt water intrusion and sea leve rise is confirmed for karst springs, for example in Bonacci and Roji-Bonacci (1997). Hence, we can assume a linear dependency of risk of salt intrusion to sea leve rise.
In Klassen et. al (2016) sea level has been considered in combination with storm surge to determine the “Designated Flood Level” (the appropriate allowance for future sea level rise, tide and the total storm surge expected during the designated flood).
Considering that the contribution of sea level rise to storm surge is included in the analysis of Storme surge projection, according with the methodology applied by Vousdoukas et al. 2016 (see section 3.2.2), in our model, the sea level component of risk to salt ingression is considered separately, in terms of its pressure on transition zone, and then combined with storm surge projection to obtain the total value of Hazard threats. The rating for sea level is then considered according to five classes (very hight, hight medium, low, very low). The sea level values associated to each class have been established based on the result of projection for Northern Adriatic basin, in the period considered, for RCP8.5.

Table 3: Ranks for vulnerability assessment for sea level rise

Class of sea level rise	Sea level rise (m)	Rating
Very Hight sea level rise	>0.209	5
Hight sea level rise	0.198 - 0.209	4

Medium sea level rise	0.188 - 0.198	3
Low sea level rise	0.177-0.188	2
Very low sea level rise	< 0.177	1

3.2.2 Storm surge

Storm surges are an important coastal hazard component and their contribution to salt intrusion in coastal aquifer is relevant. Nevertheless, the evolution of sea level storm surge along coastline in view of climate change, is not well known.

Data used here came from Vousdoukas et al. (2016). The study has used a hydrodynamic model forced by CMIP5 climate model wind and pressure fields (Taylor et al. 2011) to generate projections of extreme storm surge levels (SSL) along the European coastline, for a baseline 'historical' period and the two RCP4.5 and RCP8.5 scenarios. The return period is commonly used for risk analysis when associated to design of structure or utilities, or, as in our case, with planning of use of resources.

The relevance of a given return period for a given structure (or a given use of resources), is related to the life expectation of the structure (or use), and can be expressed by (Vogel et al., 2017):

$$\bar{R} = 1 - \left(1 - \frac{1}{T}\right)^{n} \quad (6)$$

where T is the return period and 1/T is the expression for the probability of the occurrence of the event in a year. In the case of exploitation of wells, administrative authorisations are usually related for decades (depending on water uses, but usually not less than 10 years). According to Figure 2 the maximum risk is reached for a duration of few decades (30-40 years) with a return period of 5 and 10 years.

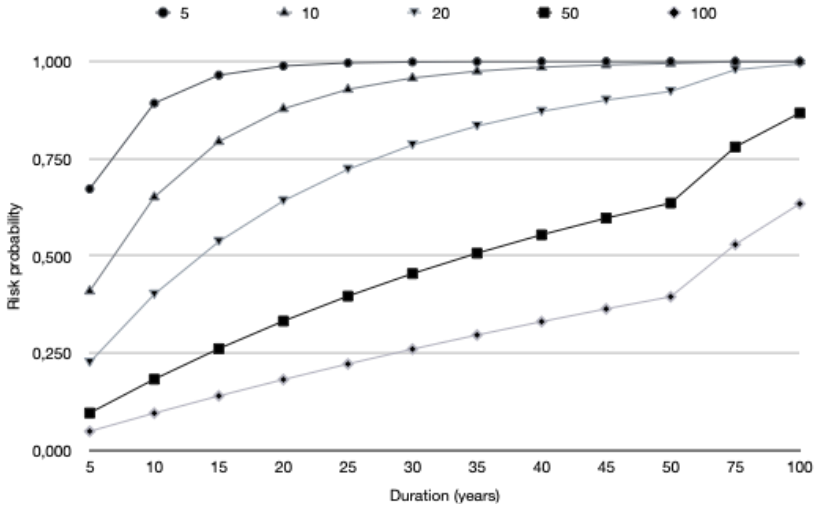

Fig 2: Relevance of return period relative to the duration of exploitation of resources

For this analysis, SSL projection according to RCP 8.5 with return period of 10 yr have been associated with our grid. The rank of SSL height is given in the table below.

Table 4: Ranks for vulnerability assessment for storm surge level (expected SSL height with a return period of 10 yr according to RCP 8.5)

Class of Storme surge level	SSL height (m)	Rating
Very Hight SSL	>2.35	5
Hight SSL	2.10-2.35	4
Medium SSL	1.85-2.10	3
Low SSL	1.60-1.85	2
Very low SSL	<1.60	1

3.2.3 Pumping

Pumping from coastal aquifers alters the natural equilibrium between seawater and freshwater. Freshwater that is discharging into the sea is intercepted and the fresh/salt-water interface migrates landward and/or locally upward. The latter is expressed as the movement of saltwater from a deeper saltwater zone into the fresh groundwater in response to pumping at a single well (Reilly and Goodman, 1987). For this reason pumping is commonly considered in risk assessment of saltwater ingression in coastal aquifer.

Eriksson et al. 2018 consider spatial distribution of wells, but do not associate a specific value of risk to different value of density. Conversely, Kennedy (2012) and Klassen et al. (2016) identify class of risk to wells density per cell unit. Kennedy (2012) distinguish domestic groundwater use and large non-domestic groundwater users: for the latter the risk is not associated to density but to volume/day of water extracted.

For this study, following the methodology proposed by Kennedy (2012) and refined by Klassen et al. (2016), we uses well density per grid unit and volume of water extracted per day.

Table 5: Ranks for vulnerability assessment for pumping

	Well density		Water extracted (m^3/d)	
Rating	**1kmx1km**	**250mx250m**	**1kmx1km**	**250mx250m**
5	>80	>20	>2000	>500
4	40 - 80	10 - 20	400-2000	100-500
3	20 -40	5 -10	40-400	10-100
2	4-20	2-5	20-40	5-10
1	1-4	1	1-20	1-5

Since the information on volume extracted are not always available, following a precautionary

approach, the rating is assigned to the worst situation between well density and water extracted.

4. Economic loss

Economic loss represents the economic consequences due to contamination of water supply. These could include different aspects, as impacts on human health or consequence to ecological systems. The main economic loss for contamination to groundwater resources are related to:

- damage to intensive business (mainly agriculture);
- costs to replace/restore water resources.

For this latter, Simpson et al. (2014) identified four potential sources of water if a well becomes contaminated; these include 1) hooking up to municipal water supply where available, 2) drilling a deeper well if the geology allows, 3) importing water, or 4) investing in another expensive long term solution such as water treatment or rainwater harvesting.

Restoration costs will depend on numerous variables, such as the possibility of replacement instead of restoration, the finale use of water (for example drinking water needs stricter quality parameter than water for industrial use, and restoration costs are higher), the availability of methods for the restoration, etc.

In general, there are a linear dependency between the quantity of water that need to be restored and the replacement/restoration coasts. The quantity of water is considered in the model as variable, with the “pumping” parameter.

In addiction to costs for substituting or restoring the resources, there are costs in term of loss of income and economic damage deriving from the non-availability of water for specific economic sectors. This is of peculiar importance for agricultural sector, that depend on availability of water.

The Corine Land Cover (CLC) map, which classifies soil uses, has been utilised as a basis for the analysis. Between the CLC classes, those which implied a potential use of water in agriculture and in industry, have been associated with a rank for the hazard, as shown in the

following table. All the other classes have been set to one.

Table 6: Ranks for Loss assessment

CLC Class (II level)	CLC Class (III level)	Rating
12 Industrial, commercial and transport units	121 Industrial or commercial units	2
21 Arable land	212 Permanently irrigated land	5
	213 Rice fields	5
22 Permanent crops	222 Fruit trees and berry plantations	4
24 Heterogeneous agricultural areas	241 Annual crops associated with permanent crops	3
	242 Complex cultivation patterns	2
	243 Land principally occupied by agriculture, with significant areas of natural vegetation	2
All other classes		1

5. Mapping the risk

The map of risk is obtained applying equation (3). For each map grid a value of risk ranging from 1 to 51 is obtained. This value does not account for pumping, that is introduced as variable for orienting planning and administrative choice.

Based on the ranks proposed in table 5, from the map of risk it is possible establish the "acceptable" level of pumping. The value of hazard threat (H_T) associated to pumping (and hence the rank for P_W in eq. 5) necessary to increment of a given value the computed risk, depend to the absolute value of the assessed risk R.

The forward problem to obtain P_W value for a given increment in total risk, at *i*-grid unitis, is given by:

$$P_{Wi} = \left(\frac{R_i + Inc}{S_{Ai} \times L_i} - H_{T-Pi} \right) \times W_{Pi}^{-1} \quad (7)$$

where Ri is the risk obtained with eq. (3) at the *i*-grid unitis (with Pw=1), $H_{T\text{-}Pi}$ is the hazard threat value obtained by equation (5) only considering the first two terms (SI and SSL) and W_{Pi} is the weight for PW in eq. (5).

In Figure 3 a simulation based on risk obtained with different combination of S_A, H_T and L from Eq. (3) has been run to obtain P_W rank necessary to increment the total risk of 5, 10 or 15 units. In general, the maximum rank of P_W =5 imply an increment of total risk only if the assessed risk has a medium value (as rule of thumb, R>15 for an increments of 5 units, R>25 for an increment of 10 and R>30 for an increment of 15). For high value of R, even low rank of P_W can contribute to an increment in total risk. For example, for R>30, in general value of P_W between 2 and 3 would increase the total risk of 10 units.

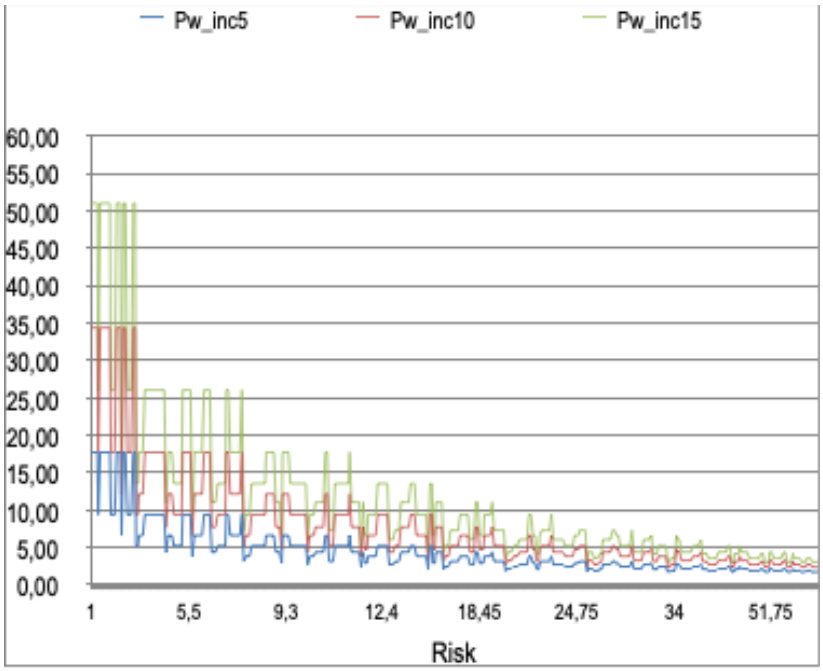

Figure 3: Theoretical value of Pw needed to obtain an increment of 5, 10 and 15 units in the total risk assessed R. "Ondulations" depend on the different value of components contributing to the assessed risk (see eq.3).

5.1 An application to the case study area of Fano

The model has been tested to the case study area of Fano (Italy).

To do that, for the Aquifer susceptibility (S_A, see Eq. 4) we have refined the information of aquifer type with the aid of the more detailed geological map of Marche Region (scale 1:10.000). A summary of the rank associated to each geological formation is listed in table 7.

Table 7: Rank to assess hydrological component of Aquifer susceptibility, scaled with the geological map of Marche region

Aquifer type	Rating	Lithology (L3)	Geology
Highly productive fissured aquifers (including karstified rocks)	5	Gravel Limestones Limestones and marls Marbles	Ancient landslide deposits; landslide deposits,
High productive aquifer	4	Quartzites Sands	Current alluvial deposits; terraces alluvial deposits; current beach deposit; Ancient beach deposit; deposit of conoid; eluvio-colluvial deposit
Low and moderately productive fissured aquifers (including karstified rocks) Low and moderately productive porous aquifers	3	Marlstones and sands Sandstones and marls	
Locally aquiferous rocks, porous or fissured	2	Clays Sandstones and clays	Colombacci formation, San Donato Formation; Gruppo Gessoso-Solfifera; Pelitic-arenaceous lithofacies; Member of the Borello Sandstones
Practically non-aquiferous rocks, porous or fissured	1		Argille Azzurre formation

The elevation has been verified using a DTM at 1:10000 scale. For the other parameters (distance from coast, sea level rise, storm surge projections and soil use) the same input data used for the general map has been put in the model.

The risk has been assessed for two different grids, the one 1km x 1km used for the general map and a more refined one with a spacing of 250x250 m. Results are shown in Figures 5 and 6.

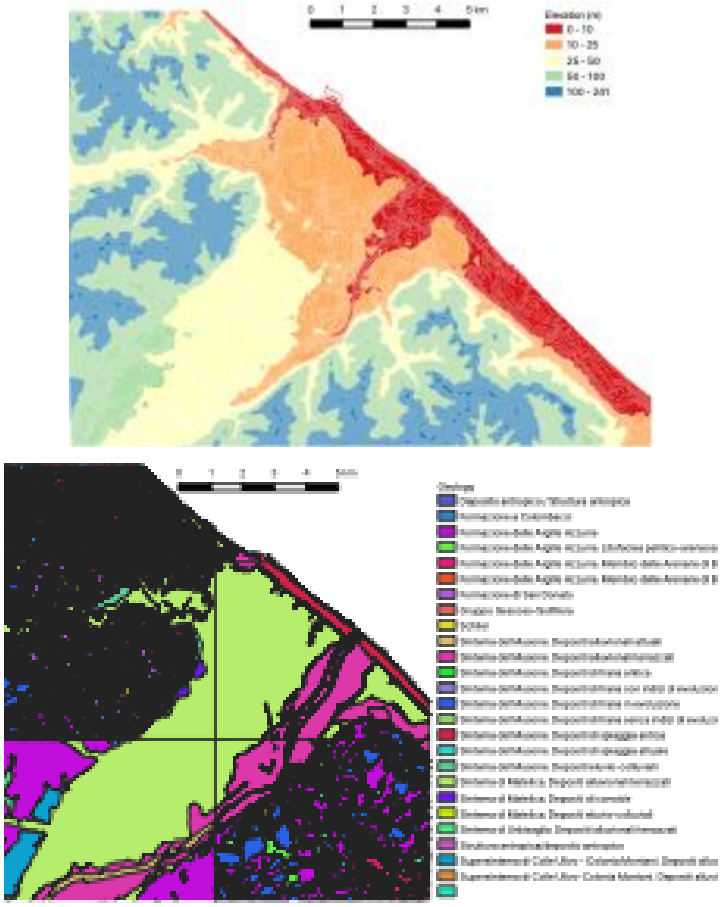

Figure 4: Case study area of Fano: elevation according to the DTM 1:10.000 (left frame) and geology map 1:10.000 (right frame)

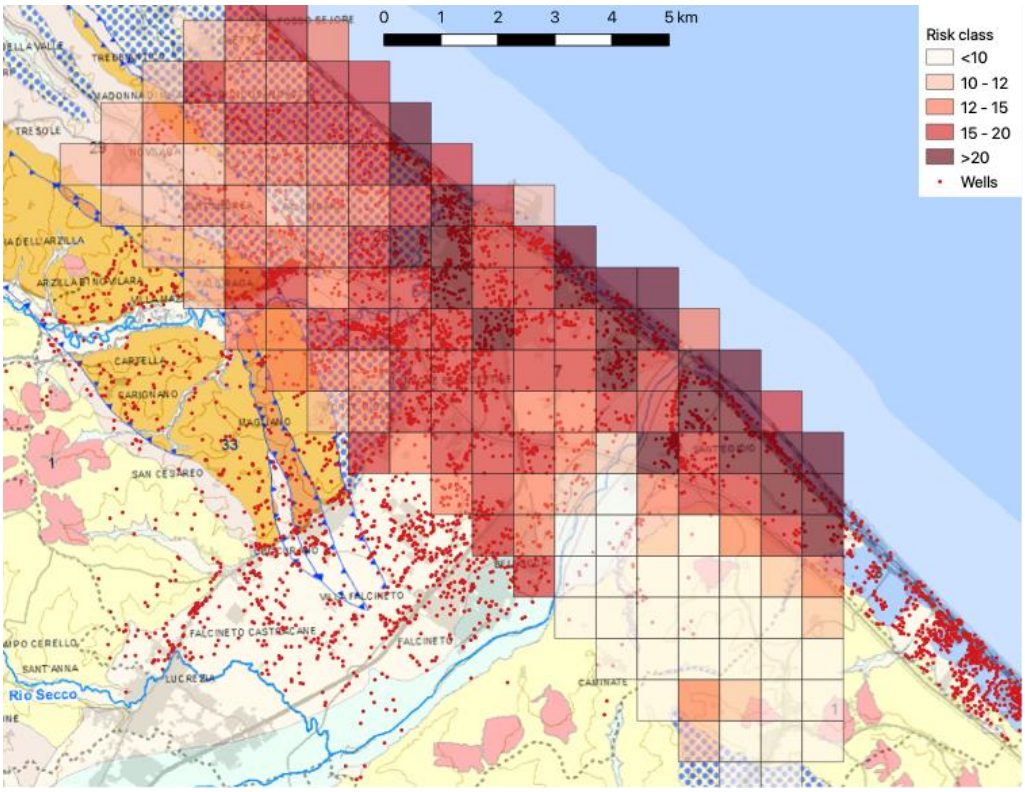

Figure 5: Case study area of Fano: risk of salt ingression on a grid 1km x 1km. Red dots mark the position of known wells. The black squares evidence the cell grids used to analyse risk variation in function of Pw (cell-A at North, cell-B at South).

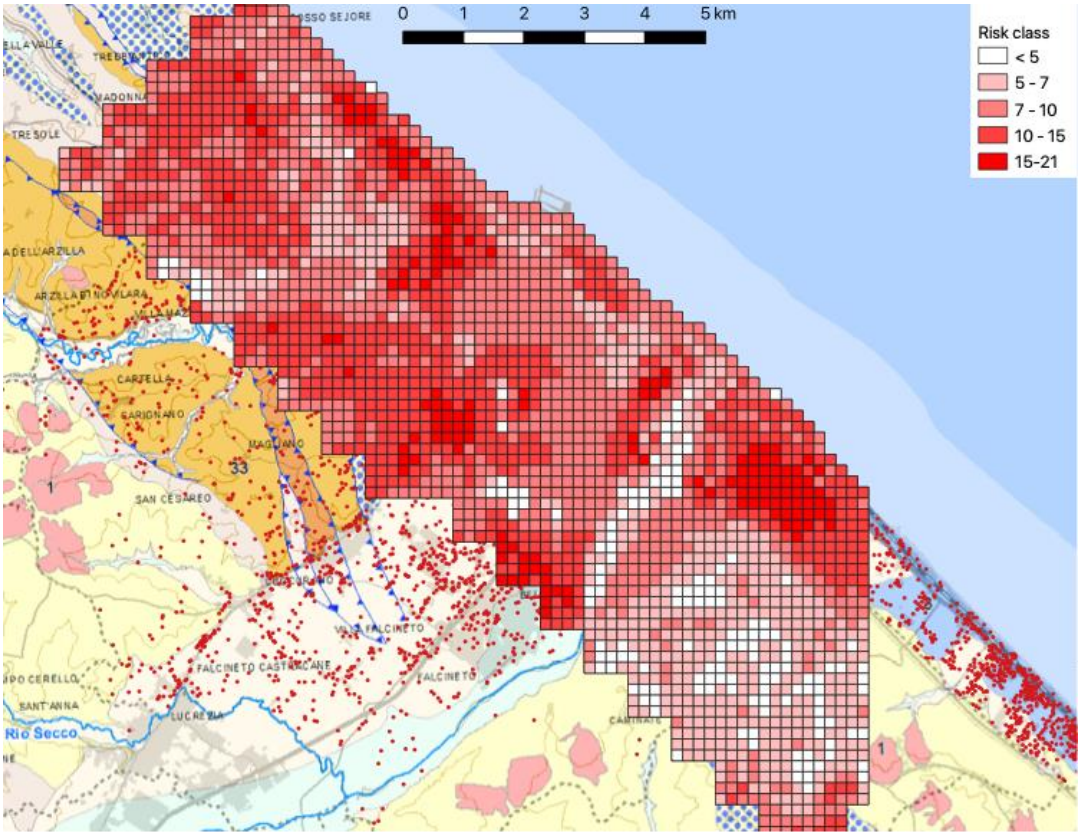

Figure 6: Case study area of Fano: risk of salt ingression on a grid 250 m x 250 m.

Available data show a concentration of wells in the Metauro River alluvial plan, with value in few cases greater than 40 wells per square km (and only in one case greater than 80). To understand the variation of risk in function of density of wells (or volume of water extraction) we have considered as an example two single grid cells, in (the black squares in Figure 5). For the northern cell (cell-A), the risk in the map (assumption Pw=1) is R=16.8, whereas for the southern cell (cell-B) R=15.6. Applying the correct rank for known weals (Pw=3, with 46 wells), the risk for cell-A became R=23.1 for cell-A . In cell-B the assessed risk remain R=15.6, since the cell actually have Pw=1 (1 wells).

The map represent a tool for the administration in the decision of authorising further water extraction and in comparing different locations. For example, authorising 10 wells in cell-B

would increase the risk, but remaining under the risk value of cell-A. An increase of risk in cell-A, up to the maximum value of R=25.2, is possible with the authorisation of 34 wells (or with an overall volume of exploitation greater than 2000 m3 per day).

REFERENCES

Bonacci, Ognjen, and Tanja Roje-Bonacci. "Sea water intrusion in coastal karst springs: example of the Blaž Spring (Croatia)." Hydrological sciences journal 42.1 (1997): 89-100.

Collins, M., R. Knutti, J. Arblaster, J.-L. Dufresne, T. Fichefet, P. Friedlingstein, X. Gao, W.J. Gutowski, T. Johns, G. Krinner, M. Shongwe, C. Tebaldi, A.J. Weaver and M. Wehner, 2013: Long-term Climate Change: Projections, Commitments and Irreversibility. In: Climate Change 2013: The Physical Science Basis. Contribution of Working Group I to the Fifth Assessment Report of the Intergovernmental Panel on Climate Change [Stocker, T.F., D. Qin, G.-K. Plattner, M. Tignor, S.K. Allen, J. Boschung, A. Nauels, Y. Xia, V. Bex and P.M. Midgley (eds.)]. Cambridge University Press, Cambridge, United Kingdom and New York, NY, USA. AR5 Cap 12

Eriksson, Marcus, Karin Ebert, and Jerker Jarsjö. "Well Salinization Risk and Effects of Baltic Sea Level Rise on the Groundwater-Dependent Island of Öland, Sweden." Water 10.2 (2018): 141.

Farrell, W. E., and James A. Clark. "On postglacial sea level." Geophysical Journal International 46.3 (1976): 647-667.

Galassi, G., and G. Spada. "Sea-level rise in the Mediterranean Sea by 2050: Roles of terrestrial ice melt, steric effects and glacial isostatic adjustment." Global and Planetary Change 123 (2014): 55-66.

Kennedy, G. W. Development of a GIS-based approach for the assessment of seawater intrusion vulnerability in Nova Scotia. 2012.

Klassen, J., and D. M. Allen (2016). "Risk of saltwater intrusion in coastal bedrock aquifers: Gulf islands, bc." Department of Earth Sciences, Simon Fraser University.

Mitrovica, Jerry X., Glenn A. Milne, and James L. Davis. "Glacial isostatic adjustment on a rotating earth." Geophysical Journal International 147.3 (2001): 562-578.

Peltier, R., Argus, D., & Drummond, R. (2013). The new ICE-6G (VM5a) model of the Global Process of Glacial Isostatic Adjustment. In EGU General Assembly Conference Abstracts(Vol.

15).

Reilly, T. E., and A. S. Goodman. "Analysis of saltwater upconing beneath a pumping well." Journal of Hydrology 89.3-4 (1987): 169-204.

Ruti, Paolo M., et al. "MED-CORDEX initiative for Mediterranean climate studies." Bulletin of the American Meteorological Society 97.7 (2016): 1187-1208.

Simpson, W.M., Allen, D.M. and Journeay, M.M. (2014) Assessing risk to groundwater quality using an integrated risk framework. Environmental Earth Science Journal 71 (11), 4939-4956.

Slangen, A. B. A., Carson, M., Katsman, C. A., Van de Wal, R. S. W., Köhl, A., Vermeersen, L. L. A., & Stammer, D. (2014). Projecting twenty-first century regional sea-level changes. Climatic Change, 124(1-2), 317-332.

Slangen, A. B. A., and R. S. W. Van De Wal. "An assessment of uncertainties in using volume-area modelling for computing the twenty-first century glacier contribution to sea-level change." The Cryosphere 5 (2011): 1655-1695.

Spada, Giorgio, J. L. Bamber, and R. T. W. L. Hurkmans. "The gravitationally consistent sea-level fingerprint of future terrestrial ice loss." Geophysical Research Letters 40.3 (2013): 482-486.

Spada, Giorgio, and Daniele Melini. "SELEN4 (SELEN version 4.0): a Fortran program for solving the gravitationally and topographically self-consistent Sea Level Equation in Glacial Isostatic Adjustment modeling." Geoscientific Model Development 12.12 (2019): 5055-5075.

Taylor, Karl E., Ronald J. Stouffer, and Gerald A. Meehl. "An overview of CMIP5 and the experiment design." Bulletin of the American meteorological Society 93.4 (2012): 485-498.

Verrjuit, Arnold (1968). "A note on the Ghyben-Herzberg formula"(PDF). Bulletin of the International Association of Scientific Hydrology. Delft, Netherlands: Technological University. 13 (4): 43–46

Vogel, Richard M., and Attilio Castellarin. "Risk, reliability, and return periods and hydrologic design." Handbook of Applied Hydrology; Singh, VP, Ed.; McGraw-Hill Book Company: New York, NY, USA (2017).

Vousdoukas, Michalis I., et al. "Projections of extreme storm surge levels along Europe." Climate Dynamics 47.9 (2016): 3171-3190.

Werner, Adrian D., and Craig T. Simmons. "Impact of sea-level rise on sea water intrusion in coastal aquifers." Groundwater 47.2 (2009): 197-204.

6. Regional High-Resolution Map of Vulnerability

Based on the results of the conceptual model of the risks, the map will show the Adriatic coastal aquifers vulnerability to salt ingression according to different scenarios of climate change. The map represents a tool for the administration in the decision of authorising further water extraction and in comparing different locations.